Brain Topography, Volume 18, Number 1, Fall 2005 (©2005)
DOI: 10.1007/s10548-005-7896-x

Multi-Resolution FOCUSS: A Source Imaging Technique Applied to MEG Data

J.E. Moran*, S.M. Bowyer*^, and N. Tepley*+

Summary: A variety of techniques are available for imaging magnetoencephalographic (MEG) data to the corresponding cortical structures. Each performs a functional optimization that includes mathematical and physical restrictions on source activity. Unlike other imaging techniques, MR-FOCUSS (Multi-Resolution FOCal Underdetermined System Solution) utilizes a wavelet statistical operator that allows spatial resolution to be chosen appropriately for focal or extended sources. Control of focal imaging properties is achieved by specifying P in an l_p norm distribution template used to construct the wavelets. In addition, incorporation of a multi-resolution wavelet operator desensitizes the mathematical algorithm to noise, (regularization). Like the FOCUSS imaging technique, an initial estimate of cortical activity is recursively enhanced to obtain the final high resolution imaging results. Studies of model MEG data representing all regions of a realistic cortical model are performed to quantify MR-FOCUSS imaging properties. These modeled data studies included single and multiple dipole sources as well as an extended source model. Thus, MR-FOCUSS is found to be very effective for imaging language processing for pre-surgical planning and provides a high-resolution method to image sequential activation of multiple correlated sources involved in language processing.

Key words: MR-FOCUSS; Magnetoencephalography; MEG; Multiresolution wavelets; Functional imaging; Language mapping.

Introduction

The relationship between MEG sensor amplitudes and amplitudes of the underlying brain electric sources is:

$$\mathbf{b}=\mathbf{b}_s+\mathbf{n}-\mathbf{G}\mathbf{q}_s+\mathbf{n} \quad (1)$$

The MEG data, **b**, is a column vector of M sensor amplitudes, which are mixtures of signal, $\mathbf{b}_s$, and noise, **n**. The sources of the signals and their amplitudes, $\mathbf{q}_s$, are not known. Assuming there are N sources, the column vectors of the M by N forward model gain matrix, **G**, relate the M sensor array measurements to the N sources in units of magnetic measurement amplitude per unit of source amplitude. For a specific array of sources, components of the gain matrix, **G**, can be accurately calculated using a multi-sphere head model matched to local variation of the skull curvature (Leahy et al. 1998; van den Broek et al. 1998; Uitert and Van Johnson 2002). However, for deep brain sources, it may be necessary to utilize a realistic head model derived from anatomical magnetic resonance imaging (MRI) studies (Mosher et al. 1999). Equation 1 is converted to a spatio-temporal equation by replacing vectors, **b** and $\mathbf{q}_s$, with matrices, **B** and $\mathbf{Q}_s$, whose columns correspond to successive time points.

Equation 1 is insufficient for determining the source amplitudes, $\mathbf{q}_s$, because only **b** is known. As a supplement to Equation 1, two relatively distinct mathematical models of brain activity are utilized. A multiple current dipole model of brain activity (Hämäläinen et al. 1993) is based on the discrete mapping of function to a few small, focal regions of cortex. These active regions are modeled as current dipoles whose locations, orientations and amplitudes must be determined. Alternatively, neuronal activity is treated as a current density continuum that is modeled by a large lattice of dipole sources within the gray mater of the brain (Hämäläinen et al. 1993).

Constraining imaged brain activity to combinations of a few independent compact sites may be inappropriate for studies of complex mental tasks, pathological activity, and sleep (Darvas et al. 2004). For these imaging applications, a continuum model brain electric activity accommodates extended and compact sources that may be simultaneously active. Using either model, brain elec-

* Henry Ford Hospital, Detroit, Michigan USA.
+ Oakland University, Rochester Michigan USA.
^ Wayne State University, Detroit, Michigan, USA.
Accepted for publication: July 22, 2005.
This research including the development of the MR-FOCUSS imaging technique and software implementation was supported by NIH/NINDS Grant R01 NS30914.
Correspondence and reprint requests should be addressed to John E. Moran, Ph.D., Henry Ford Hospital, MEG Laboratory CFP78/79, 2799 W. Grand Blvd., Detroit, MI, 48202-2689, USA.
Fax: 313-916-0526
E-mail: moran@neurnis.neuro.hfh.edu

tric activity is estimated by minimizing (maximizing) an imaging metric that includes contributions of individual brain electric sources proportional to their participation in the collective fulfillment of equation 1 as well as other source activity constraints. Ideally, these constraints are derived from prior knowledge of brain activity.

A current density imaging filter is constructed by minimizing the norm of weighted source amplitudes with Equation 1 as a constraint. A prototype current density imaging filter, **H** (Baillet et al. 2001; Liu et al. 2002), is applied to MEG data, **b**, to obtain an estimate of cortical activation, $\mathbf{q}_{estimate}$:

$$\mathbf{q}_{estimate} = \mathbf{Hb}$$

$$\mathbf{H} = \mathbf{WW}^T\mathbf{G}^T\left[\mathbf{GWW}^T\mathbf{G}^T + \Phi(\mathbf{nn}^T)\right]^{-1}$$

$\Phi(\mathbf{nn}^T)$ is a regularization function such as $\lambda\mathbf{I}$ (2)

The matrix, **W**, is an estimate of source activity that has a covariance matrix, $\mathbf{WW}^T$. The matrix $\mathbf{GWW}^T\mathbf{G}^T$ is an estimate of the signal covariance matrix. The spatial resolution of imaged activity is good only when $\mathbf{WW}^T$, is an accurate estimate of the source covariance matrix. A popular choice for $\mathbf{WW}^T$ is the identity matrix, **I**. This is a very poor source covariance estimate for imaging focal source activity.

Methodologies have been developed for altering the covariance matrix, $\mathbf{WW}^T$, to address current density imaging blur. One method with great potential utilizes corresponding functional MRI (fMRI) results to estimate the source covariance matrix, $\mathbf{WW}^T$ (Dale et al. 2000; Liu et al. 1998). However, the efficacy of this approach is limited because the mathematical relationships between MEG imaged activity and fMRI imaged activity are poorly established (Horwitz and Poeppel 2002). Another approach uses the MEG imaging results of equation 2 to recursively update the estimated source covariance matrix, $\mathbf{WW}^T$. The Focal Underdetermined System Solver (FOCUSS) imaging technique (Gorodnitsky et al. 1995; Gorodnitsky and Rao 1997) uses this recursive update strategy to enhance imaging compact sources. The algorithm was shown to generate a sparse solution in which a few sources, (less than the number of MEG sensors), have nonzero amplitudes (Gorodnitsky et al. 1995). Localization accuracy of FOCUSS is improved when the algorithm is initialized with a source covariance matrix, $\mathbf{WW}^T$, based on prior knowledge of the estimated source activity (Gorodnitsky and Rao 1997; Rao and Kreutz-Delgado 1999). Additional control of focal imaging is obtained by formulating the FOCUSS technique as a constrained minimization of a diversity measure, $E^P(\mathbf{q}) = \|\mathbf{q}\|^P$, which is the l_p norm of **q**. This imposes a constraint on the statistical distribution of cortical source amplitudes (Rao et al. 2003). The exponent, P, controls focal sparseness of solutions constructed by minimizing $E^P(\mathbf{q})$. Imaged activity has fewer nonzero source amplitudes when P is close to 0.

A different recursive imaging strategy utilizes threshold elimination of low amplitude sources from the cortical model combined with increased source grid density in high amplitude regions. Thus, a sequence of cortical models is generated that progressively confines imaged activity to regions of smaller size but increased spatial resolution (Okada et al. 1992; Gavit et al. 2001). Compared to the FOCUSS technique, elimination of low amplitude sources increases the computational efficiency. Also, spatial and temporal constrains are used to minimize noise sensitivity of the algorithm (Gavit et al. 2001). Unfortunately, recursive threshold elimination techniques can become unstable especially when the signal-to-noise ratio is low.

Recursively applied current density imaging techniques incorporate two mathematical features important for high resolution MEG source imaging. First, it is relatively easy to incorporate prior knowledge of brain activation obtained using other MEG imaging techniques or other imaging modalities such as fMRI. Second, they are capable of high-resolution imaging of compact source activity as well as extended regional activation.

We developed the current density imaging technique, MR-FOCUSS to alleviate the noise instability problem associated with recursive algorithms for MEG imaging. In MR-FOCUSS, the dipole grid of cortical sources is transformed into a multiresolution wavelet model of the cortex. In this source basis, the signal content of the data is preferentially imaged using high spatial resolution wavelets while noise is excluded. In contrast, noise is weakly coupled to the lowest resolution wavelet structures, which act as low-pass spatial filters. The small amount of noise incorporated in these wavelets is spread over large regions at very low amplitude. This wavelet source basis is shared with our 2DII imaging technique (Moran and Tepley 2000). However, MR-FOCUSS is significantly faster than 2DII because the wavelet subspace basis vectors are calculated once for all MEG data that is imaged and MR-FOCUSS converges in significantly fewer steps than 2DII. Further, MR-FOCUSS enables the focal imaging properties of the algorithm to be selected by specifying the l_p norm of an imaging metric used to construct the wavelet source template. This method of focal imaging control is similar to the choice of the l_p norm controlling image sparseness in the FOCUSS algorithm (Rao et al. 2003).

Methods

MR-FOCUSS Imaging Algorithm

MR-FOCUSS iteratively updates an estimate of cortical source amplitudes, $\mathbf{q}^{(i)}$, (the superscript corresponds to the step number within the iterative solution sequence). The forward calculated sensor amplitudes are $\mathbf{b}^{(i)} = \mathbf{G}\mathbf{q}^{(i)}$ for the source distribution, $\mathbf{q}^{(i)}$. The residual vector, $\mathbf{r}^{(i)}$, is the difference between the data, $\mathbf{b}$, and $\mathbf{b}^{(i)}$. Starting with an initial estimate of source activity, $\mathbf{q}^{(0)}$, the goal of the MR-FOCUSS algorithm is to construct a source structure estimate, $\mathbf{q}^{(i+1)}$, such that $\mathbf{r}^{(i+1)}$ is a good estimate of the noise, $\mathbf{n}$. The noise, $\mathbf{n}$, is assumed to be spatially uncorrelated with the signal, $\mathbf{b}_S$, and with all the forward calculated signals in the gain matrix, $\mathbf{G}$, of active cortical sources. The imaging algorithm constructs the vector, $\mathbf{b}^{(i)}$, by projecting the data, $\mathbf{b}$, onto a multi-resolution solution subspace, $\mathbf{G}_P$, with $\mathbf{r}^{(i)}$ in the null space of $\mathbf{G}_P$. Therefore, $\mathbf{b}^{(i)}$, which estimates $\mathbf{b}_S$, is orthogonal to the residual $\mathbf{r}^{(i)}$, which estimates the noise, $\mathbf{n}$, and the inner product of these vectors can be rewritten as the inner product of two orthogonal source vectors, $\mathbf{q}^{(i)}$ and $\mathbf{q}_r^{(i)}$.

$$\mathbf{b}^{(i)T}\mathbf{r}^{(i)} = \mathbf{q}^{(i)T}\mathbf{G}^T\mathbf{r}^{(i)} = \mathbf{q}^{(i)T}\mathbf{q}_r^{(i)}$$
$$= \sum_{k=1}^{N}\left[q^{(i)}q_r^{(i)}\right]_k = \sum_{k=1}^{N}\left[q_{rq}^{(i)}\right]_k = 0 \text{ with } \mathbf{q}_r^{(i)} = \mathbf{G}^T\mathbf{r}^{(i)} \quad (3)$$

The weighted correlation vector, $\mathbf{q}_{rq}^{(i)} = \text{diag}(\mathbf{q}^{(i)})\,\mathbf{q}_r^{(i)}$ is composed of the element by element products of the vectors, $\mathbf{q}^{(i)}$ and $\mathbf{q}_r^{(i)}$. The vector $\mathbf{q}_{rq}^{(i)}$ incorporates both source amplitudes and correlations between signals of sources and the residual. From equation 3, the probability density distribution of the amplitudes of $\mathbf{q}_{rq}^{(i)}$ has a mean of zero.

Control of the focal imaging properties is introduced by modeling the probability density distribution of the components of $\mathbf{q}_{rq}^{(i)}$ with the function:

$$p\left(q_{rq}^{(i)}\right) = C\,e^{-\frac{\left\|f\left(q_{rq}^{(i)}\right)\right\|^2}{2\beta^2}} \quad (4)$$

The function $f(\mathbf{q}_{rq}^{(i)}) = \mathbf{P}\mathbf{P}^T\mathbf{q}_{rq}^{(i)}$, includes the multiresolution statistical operator, $\mathbf{P}\mathbf{P}^T$.

The matrix $\mathbf{P}$ contains a set of 8 multiresolution wavelet vectors, which are constructed using a statistical density distribution template, $\mathbf{M}_P(z) = \left[Ae^{-|z^P|}, 0 \le p \le 2\right]$.

The exponent P of the distribution controls the focal imaging properties of MR-FOCUSS. The focal imaging parameter, P, is an input parameter of the MR-FOCUSS algorithm. The wavelet matrix is designated with the letter, $\mathbf{P}$, because the wavelet vectors incorporate the statistical properties corresponding to the parameter, P, into the MR-FOCUSS solution. Details of constructing $\mathbf{M}_P(z)$ and multiresolution wavelet matrix, $\mathbf{P}$, are in the appendix. Prior to multiplication by the operator, $\mathbf{P}\mathbf{P}^T$, the statistical operator, $f(\mathbf{q}_{rq}^{(i)})$, alters the order index, k, of the elements of the vector, $\mathbf{q}_{rq}^{(i)}$, such that these elements are placed in rank order (most negative to most positive). The rank ordered index of each source is related to the old index by [rank_index = f(k)].

$$f\left(\left[q_{rq}^{(i)}\right]_k\right) \xrightarrow{\text{place in rank order}} \left[q_{rq}^{(i)}\right]_{\text{rank\_index}}$$
$$\text{rank\_index} = f(k) \quad (5)$$

In equation 6, the relationships between $\mathbf{q}_{rq}^{(i)}$ and, $\mathbf{q}^{(i)}$ and $\mathbf{q}^{(i+1)}$ and the columns of the gain matrix, $\mathbf{G}$ are maintained by their rearrangement and use in all following equations.

$$\left[q^{(i)}\right]_k \rightarrow \left[q^{(i)}\right]_{\text{rank\_index}}$$
$$\left[q^{(i+1)}\right]_k \rightarrow \left[q^{(i+1)}\right]_{\text{rank\_index}}$$
$$[g_x, g_x, g_x]_k \rightarrow [g_x, g_x, g_x]_{\text{rank\_index}} \quad (6)$$

The residual, $\mathbf{r}^{(i)}$ estimates the noise, $\mathbf{n}$, when $\mathbf{q}^{(i+1)}$ maximizes the probability that all elements of $\mathbf{q}_{rq}^{(i)}$ are zero.

$$\mathbf{q}^{(i+1)} = \arg\max \log\, p\left(\left\langle q_{rq}^{(i)}\right\rangle = 0\right) \Leftrightarrow$$
$$\mathbf{q}^{(i+1)} = \arg\min \left\| f\left(q_{rq}^{(i)}\right)\right\|^2 \quad (7)$$

After applying $f(\mathbf{q}_{rq}^{(i)})$ in equations 5 and 6:

$$\mathbf{q}^{(i+1)} \text{ that minimizes } \left\|\mathbf{P}\mathbf{P}^T\mathbf{q}_{rq}^{(i)}\right\|^2 = \mathbf{q}_{rq}^{(i)T}\mathbf{P}\mathbf{P}^T\mathbf{P}\mathbf{P}^T\mathbf{q}_{rq}^{(i)} =$$
$$\mathbf{q}_{rq}^{(i)T}\mathbf{P}\mathbf{P}^T\mathbf{q}_{rq}^{(i)} \text{ with wavelet basis vectors } \Rightarrow$$
$$\mathbf{P} = [p_0, p_1, \ldots, p_7] \quad \mathbf{P}^T\mathbf{P} = \mathbf{I} \quad (8)$$

Next $\mathbf{q}_{rq}^{(i)}$ is replaced with $\text{diag}(\mathbf{q}^{(i)})\mathbf{G}^T\mathbf{r}^{(i)}$ to obtain:

$\mathbf{q}_Q^{(i+1)}$ that minimizes

$$\left[\mathbf{b}^T\mathbf{G}_Q - \mathbf{q}_Q^{(i+1)}\mathbf{G}_Q^T\mathbf{G}_Q\right]\left[\mathbf{G}_Q^T\mathbf{b} - \mathbf{G}_Q^T\mathbf{G}_Q\,\mathbf{q}_Q^{(i+1)}\right]$$

with:

$$\mathbf{r}^{(i+1)^T} = \mathbf{b}^T - \mathbf{q}_Q^{(i+1)}\mathbf{G}_Q^T$$

$$\mathbf{G}_Q = \mathbf{G}\,\mathrm{diag}(\mathbf{q}^{(i)})\mathbf{P} = \mathbf{G}\mathbf{Q}$$

$$\mathbf{Q} = \mathrm{diag}\left(\mathbf{q}^{(i)}\right)\mathbf{P}$$

$$\mathbf{q}^{(i+1)} = \mathbf{Q}\mathbf{q}_Q^{(i+1)} \qquad (9)$$

The solution of equation 9 is a least-squares solution for the multiresolution source amplitudes:

$$\mathbf{q}_Q^{(i+1)} = \left[\mathbf{G}_Q^T\mathbf{G}_Q\right]^{-1}\mathbf{G}_Q^T\mathbf{b}$$

$$\mathbf{q}^{(i+1)} = \mathbf{Q}\mathbf{q}_Q^{(i+1)} = \mathrm{diag}\left(\mathbf{q}^{(i)}\right)\mathbf{P}\mathbf{q}_Q^{(i+1)} \qquad (10)$$

In our implementation of MR-FOCUSS, the matrix inversion in equation 10 is avoided by a conjugate gradient solution (Moran and Tepley 2001) of $\mathbf{G}_Q^T\mathbf{b} = \mathbf{G}_Q^T\mathbf{G}_Q\,\mathbf{q}_Q^{(i+1)}$ for the source amplitudes, $\mathbf{q}_Q^{(i+1)}$. Note the source estimate, $\mathbf{q}^{(i+1)}$, is a modification of the source estimate of the previous step, $\mathbf{q}^{(i)}$, because the first column vector of the matrix, $\mathbf{Q}$, is $\sqrt{N}\mathbf{q}^{(i)}$ where N is the number of cortical model sources. Therefore, an MR-FOCUSS solution includes an attenuated version of the initial source estimate.

The solution of equation 10 minimizes the norm of $\mathbf{q}_{rq}^{(i)}$. However, the local minimum of the norm of the residual field, $\mathbf{r}^{(i)}$ is used to determine the iteration end point of the MR-FOCUSS algorithm. This algorithm end point is used to avoid imaging noise. Usually the magnitude of both $\mathbf{q}_{rq}^{(i)}$ and $\mathbf{r}^{(i)}$ decrease during the first 3 iterative steps. The algorithm is terminated when further modification of the initial source estimate fails to reduce the magnitude of the residual, $\mathbf{r}^{(i)}$. If the initial source estimate is very poor, the amplitude of the residual will often be large. The dependence of MR-FOCUSS solutions on the initial estimate of source activity is shared with other current density imaging techniques (Baillet et al. 2001; Liu et al. 1998; Liu et al. 2002; Dale et al. 2000). Averaging multiple MR-FOCUSS solutions constructed from a set of initial source estimates, which differ by random perturbations of the source amplitudes can be useful for minimizing the influence of initialization bias (Moran and Tepley 2000). Other procedures can be used to extract statistically significant solution components (Schmidt et al. 1999; Hanson and Swithenby 2001; Darvas et al. 2004) from multiple biased solutions. A description of the single current dipole metric used for source initialization of MR-FOCUSS solutions presented in this paper is included in the appendix.

Cortical Model

The MR-FOCUSS imaging technique utilizes MRI anatomical images to construct a model of the subject's cortex (Moran et al. 2001). Prior to constructing this model, the MRI (pixel) coordinates are co-registered to MEG (cm) coordinates (positive x axis through the bridge of the nose, positive y axis through the left ear canal, z axis through the top of the head). The cortical model consists of 3472 sites distributed such that each represents an equivalent amount of cortical gray mater, figure 1A. In equation 1, the columns of the gain matrix, G, are calculated using multiple spheres fit to local curvature of the skull surface. For each cortical site, three columns of G correspond to equivalent current dipoles oriented in x, y, and z directions. Cortical model construction is one module of our MEG_tools imaging software (Moran and Tepley 2005).

Modeled MEG Data

MEG sensor amplitudes were calculated for 72 simulated dipole sources located throughout a cortical model constructed from anatomical MRI volumetric data of a normal subject, figure 1B. The orientation of each source was adjusted to maximize signal power in the MEG sensor array, shown in figure 1C. In addition, source amplitudes were modified such that all had the same maximum sensor amplitude. MR-FOCUSS solutions were constructed for these signals with and without added random noise. Noise was normally distributed with mean of zero and amplitude adjusted such that the noise power was 150% of the signal power. A model of signal averaged MEG data was created by combining the signal of a right anterior dipole source with an average of 100 epochs of MEG sensor noise including environmental artifact.

For these data the MEG sensor noise averaged 17 % of the dipole signal power. In addition, MR-FOCUSS solutions were constructed for an extended source model that was created by summing MEG sensor amplitudes from 270 cortical model sites.

Language Processing Study

MR-FOCUSS was used to image MEG recordings of cortical activity acquired while a verb generation task was performed by subjects. The focal imaging parameter was P = 0.6 and amplitudes above 20% of maximum amplitude were included in the final solutions. Twenty solutions were averaged for each time point with the initial estimate of cortical activity consisted of random amplitudes (Moran and Tepley 2000). The mean initialization amplitude of sources is zero with random source initialization. Therefore, imaging error associated with a sin-

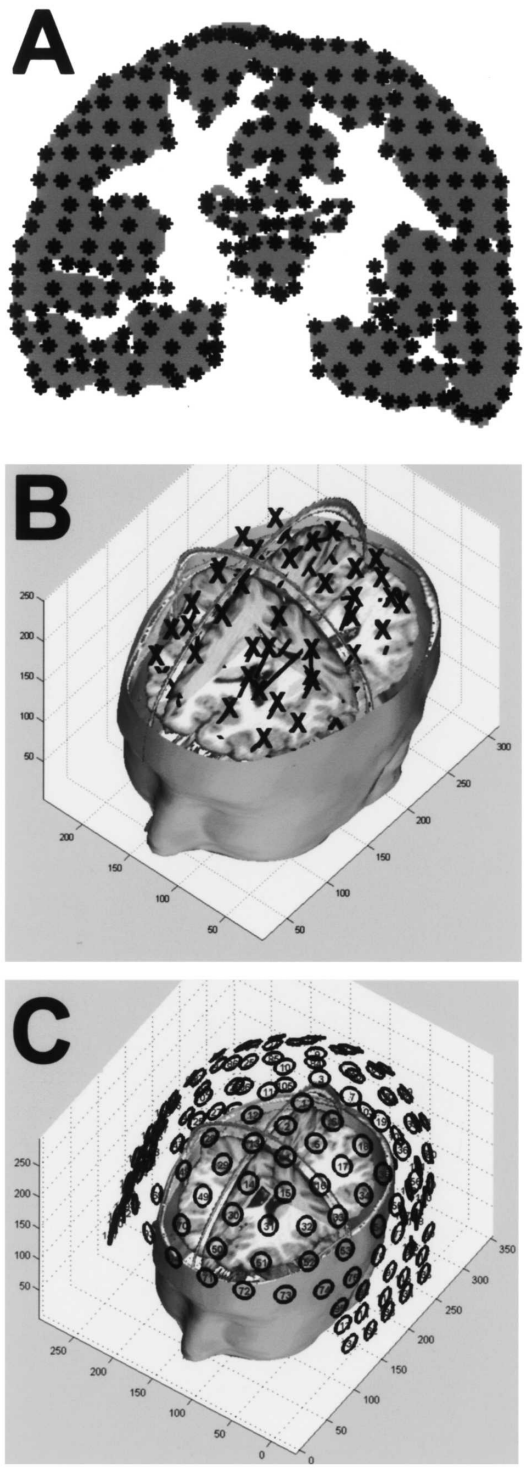

Figure 1. (A) The forward model was calculated for 3472 locations distributed to match the cortical gray matter, as shown in this figure. (B) The 72 dipole sources are uniformly distributed within the cortical gray mater with orientations that maximize signal power in the MEG sensor array. (C) The proximity of the MEG sensor array to the cortical model is shown.

gle poor source estimate is avoided. Further, imaging low amplitude source activity is often enhanced because high amplitude sources have low initialization weights in some of the 20 solutions. However, MR-FOCUSS images constructed with this initialization strategy retain a small amount of random initialization noise (see discussion following equation 10).

In this study, epochs of MEG data were recorded for eighty presentations of concrete nouns [every day objects]. During each presentation the subject silently generated a verb that was linked to the noun (example: book - read). A single average response of two seconds duration was created and band pass filtered, 3-70 Hz, with a notch filter at 60 Hz to remove electronic and patient generated artifact.

Results: Modeled Data

Statistical Significance of Source Amplitudes

MR-FOCUSS solutions were constructed with focal imaging parameters, P = [2.0, 1.0, 0.4, 0.2, 0.1, 0.05], for simulated MEG data, without noise from 72 single dipole sources, shown in figure 1. A single current dipole metric, described in the appendix, was used to initialize these MR-FOCUSS solutions. The statistical distributions of sources versus source amplitudes as a percent of the maximum source amplitude are shown in figure 2 for focal imaging parameters, P = [2.0, 0.4, 0.2 and 0.05]. Distributions for all 72 MR-FOCUSS solutions were averaged for this figure. In general, these lines are shifted upward for deep sources and down for those close to the measurement array. Usually we use a threshold of 20%of maximum amplitude for including sources in MR-FOCUSS solutions. With P = [2.0, 0.4, 0.05], these MR-FOCUSS solutions had approximately [125, 84, 36] of the 3472 sources above the 20% threshold.

Multiresolution Wavelet Operator

The mechanism by which imaging wavelets control spatial resolution is shown in figure 3. Four of eight wavelets sources from the first iteration of an MR-FOCUSS solution for a right anterior single dipole source are displayed. As this figure illustrates, the low spatial resolution wavelet alters all cortical amplitudes while the other wavelets perform a set of increasingly localized changes in source amplitudes. The amplitudes of sources colored red are altered in opposite direction as amplitude of the blue sources during the solution of equation 10. The wavelet asymmetry enables large focal changes of cortical activity to be balanced by a relatively small alteration of amplitudes across a much larger set of sources, as in figure 3B and figure 3C. During subse-

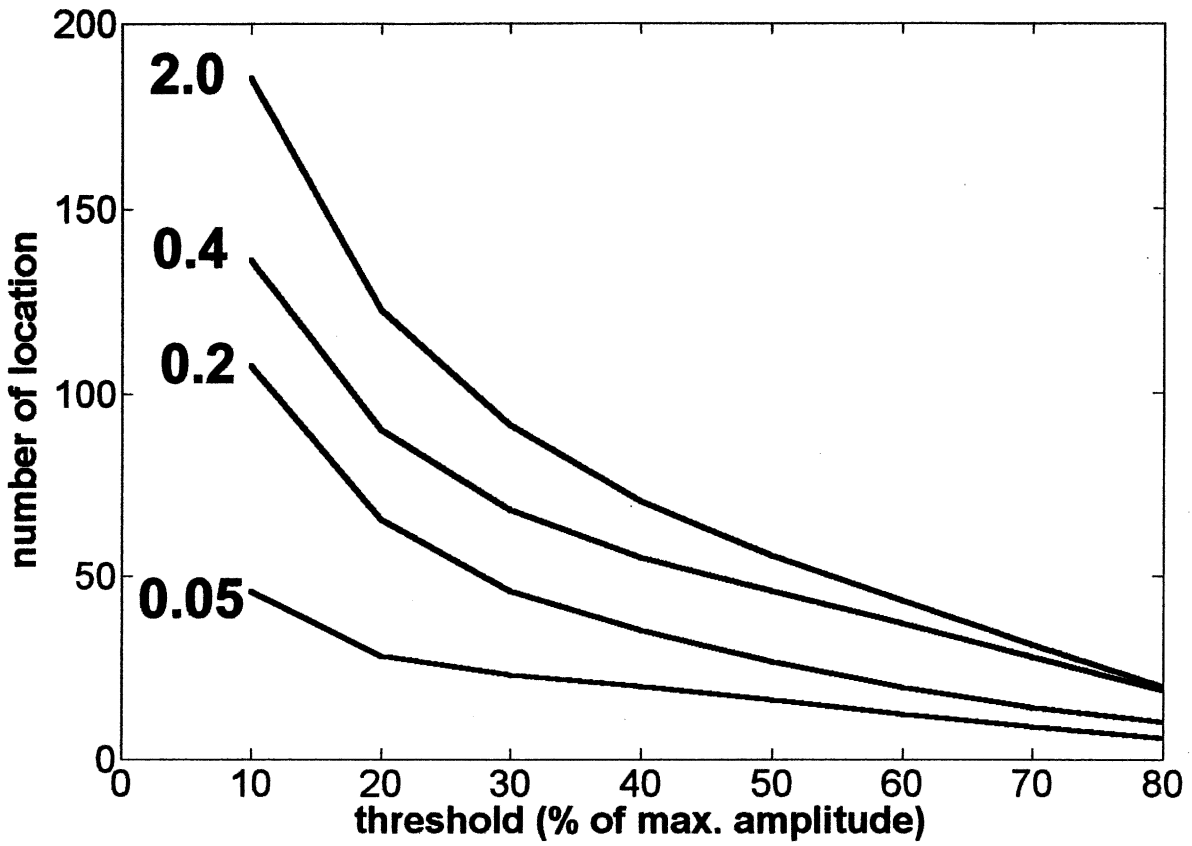

Figure 2. The relationship between the number of significantly active locations imaged by MR-FOCUSS and imaging threshold is shown in this figure. Also, the number of significant active sources is affected by the focal imaging parameter, P, which controls the statistical distribution of MR-FOCUSS solution amplitudes. For these MR-FOCUSS solutions, less than 3.6 % of the 3472 locations are above a threshold of 20% of the maximum single source amplitude.

quent iterations, all sources are reassigned to the imaging wavelets according to the rank order of imaging metric amplitudes, $\mathbf{q}_{rq}^{(i)}$. Construction of the wavelets is detailed in the appendix.

MR-FOCUSS Point Spread Function

For imaging filters, **H**, the point-spread function is quantified by the blurred image estimate, $\mathbf{q}_{estimate} = \mathbf{HGq}$ of a current dipole source, **q**, where **HG** (product of the imaging filter, **H**, and gain matrix, **G**) is the resolution matrix (Liu et al. 2002). For imaging filters, the point-spread function depends on noise regularization and how close the prior knowledge matrix, $\mathbf{WW}^T$, matches the source covariance matrix.

MR-FOCUSS does not create an imaging filter. Rather, the point-spread function of MR-FOCUSS was quantified by imaging modeled MEG data from 72 single dipole sources representing all regions of the cortical model. The MR-FOCUSS point spread depends on the focal imaging parameter, P used to construct the wavelet matrix, **P** and how closely the initial source estimate, $\mathbf{q}^{(0)}$, matches the actual source distribution.

For each MR-FOCUSS solution, the location of a source was determined by averaging the amplitude-weighted locations of all source activity above a threshold of 20%. Next, the point-spread function was quantified by determining a variance volume surrounding each location. Variance volumes are constructed by performing a principal component analysis (PCA) of the three dimensional distribution of source amplitude about the amplitude weighted location. Orientations of variance volume axes are aligned with the eigen-vectors and outer dimensions along these axes by the square root of the eigen-values of the PCA decomposition (Gavit et al. 2001). In figure 4, variance volumes are shown for MR-FOCUSS solutions constructed with imaging parameter, P = 2.0 (4A) and P = 0.05 (4B). For one of the dipole sources, the MR-FOCUSS solutions are displayed for P = 2.0 (figure 4C) and P = 0.05 (figure 4D). These solutions correspond to the green variance volume in figure 4A and 4B.

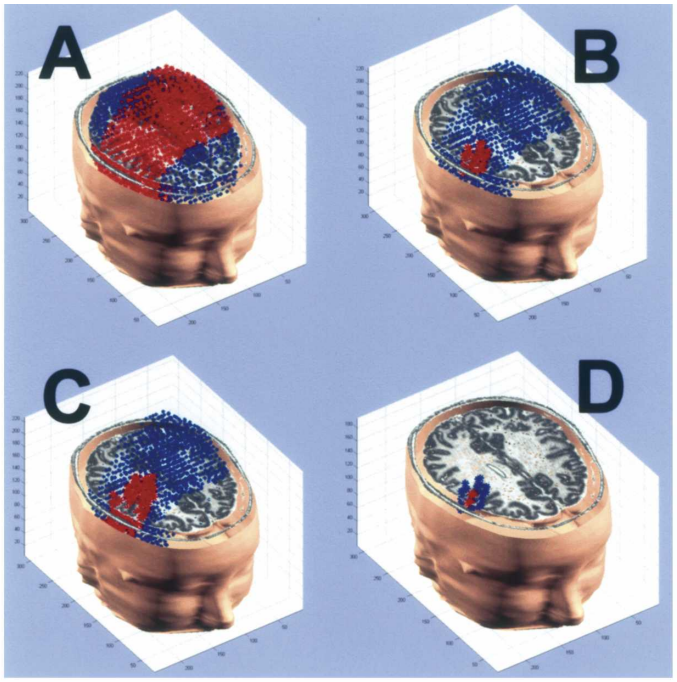

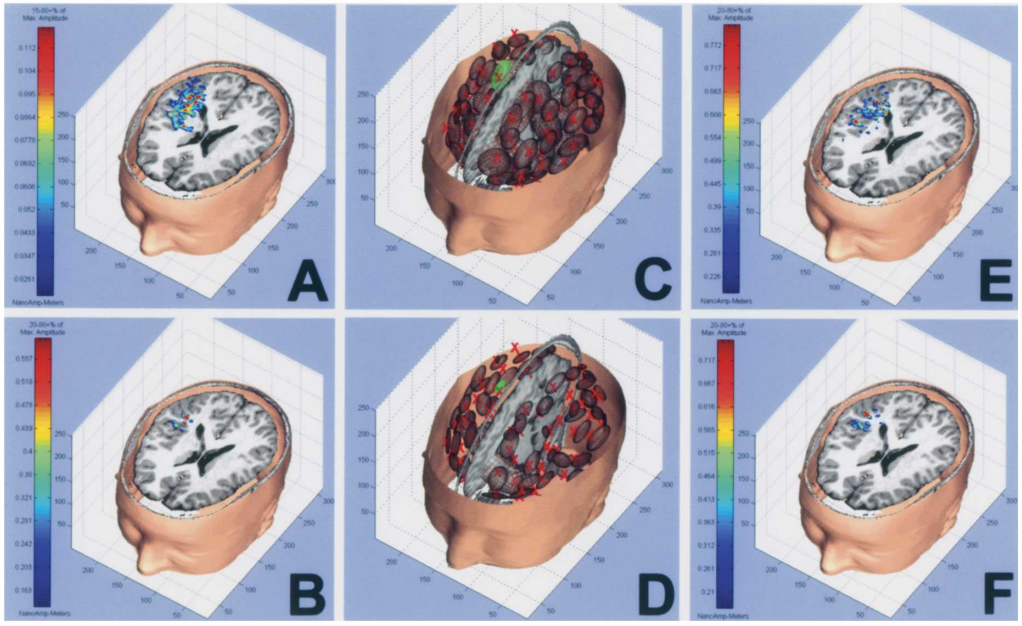

Figure 3 (Top). Four of eight imaging wavelets are depicted for imaging the signal of an anterior dipole during the first step of the MR-FOCUSS algorithm The amplitudes of red and blue sources are altered in opposite directions. The wavelet (A) performs low-resolution modifications of the entire cortical structure. In contrast, the wavelet (D) makes high-resolution modifications of source amplitudes in the vicinity of the dipole location. Wavelets, (B) and (C) alter red structure at relatively high-resolution and blue structure at low-resolution. After each iterative step, sources are reassigned as determined by the evolving imaging metric amplitudes, $\mathbf{q}_{\mathbf{rq}}^{(\mathbf{i})}$.

Figure 4 (Bottom). Source activation above a threshold of 20% of maximum single source amplitude is significantly less for MR-FOCUSS solutions with the focal imaging parameter, P = 0.05 (B and F) compared to P = 2.0 (A and E). For A and B the MEG data were free of noise. MEG data for E and F contained noise whose power was 150% of the signal power. Variance volumes for sources above 20% threshold are displayed for MR-FOCUSS solutions of noise free data from all 72 sources. The variance volumes for focal imaging parameter, P = 0.05 (D) are significantly smaller that those for P = 2.0 (C). The green variance volume corresponds to the imaged activation shown in A and B.

Dipole Localization Accuracy

The localization accuracy of MR-FOCUSS is a function of source depth, solution threshold and the focal imaging parameter used to create the solution. In figure 5, regression lines for localization error are plotted versus distance from the cortical surface for different solution thresholds. The multiple regression lines correspond to different solution thresholds between 10 and 80% of maximum amplitude with the thick regression line corresponds to a threshold of 10%. Only the extremes of focal imaging parameters, P = 2.0 (top), and P = 0.05, (bottom) are shown. Results for other focal imaging parameters are between these extremes. The correlation between the field patterns of the MEG data and corresponding field patterns of the summed activity of the MR-FOCUSS solutions was 0.996 ± 0.004. Because these are modeled data, the deterioration in performance with depth is not due to Forward model error. Rather, the location, shape and size of variance volumes (figure 4) reflect differences in x, y, an z spatial resolution of the MEG array with depth and location combined with the relative adequacy of the initial source estimate.

Sensitivity to Random Noise

In addition to signal, real MEG data contains random noise, spatially correlated noise, and artifact. MR-FOCUSS is optimized to be insensitive to random noise (see equations 7 and 8). Insensitivity of MR-FOCUSS to noise was demonstrated by imaging the MEG data for each of the 72 sources mixed with zero mean random noise such that the noise power was 120% of the signal power. On average, forward calculated fields of these MR-FOCUSS solutions excluded 51% (power) of these very noisy data and their correlation with the embedded noise free MEG data was 0.96 ± 0.04. The addition of noise increased the localization error from 7 mm to approximately 17 mm and variance volume (point spread) increased by a similar amount. Graphed in figure 6 are average imaging errors for all 72 sources, which include both surface and deep sources. The effect of added noise on the imaging results of one source are shown in figure 4E for P = 2.0 and figure 4F for P = 0.05.

Imaging Interference , Multiple Source Activity

MEG data corresponding to the combination of two dipoles can closely approximate MEG data from one source, two separate sources, or more than two sources. This increases the difficulty of generating a sufficiently accurate initial estimate of source activity.

The MEG signal from the source imaged in figure 4A was combined with the MEG signal from each of the other sources to obtain 71 sets of MEG data. MR-FOCUSS solutions were generated for these data with the initial estimate of source activity obtained using the single current dipole metric method. The localization error for each of the two sources was calculated and averaged for each solution. The number of solutions versus two source localization error is plotted in figure 7A. Included is a plot of the residual power as a percent of the data power, which is often large when MR-FOCUSS is poorly initialized. These results show that deterioration of localization accuracy is associated with a rise in the amplitude of the residual power. In figure 7B, the number of solutions versus localization accuracy is graphed for MR-FOCUSS solutions of each source imaged separately. The average localization error was 8 mm for single source imaging results and 18.3 mm for two dipole combinations.

Sensitivity to Real MEG Sensor Noise

MEG data was created by mixing the signal of a current dipole in the right temporal cortex with 210 samples of signal averaged MEG sensor noise. The noise power averaged 17% of the signal power across a range of a range of 5 to 42% . MR-FOCUSS solutions with P = [2.0 1.0, 0.2, 0.1, 0.05] were constructed for each of the 210 signal and noise mixtures. Initial source estimates were generated by the single current dipole metric described in the appendix. For these solutions, the average center of imaged activity was 1.0 cm ± 0.4 from the actual source location compared to an average localization error of 0.66 cm ± 0.3 for single current dipole imaging results. MR-FOCUSS solutions excluded a significant fraction of the noise during the imaging of these data. In figure 8A, the residual power, $\left|\mathbf{r}^{(i)}\right|^2$, of MR-FOCUSS solutions versus actual noise power is plotted. Most of the solution residual is noise. Therefore, in figure 8B, the correlation of forward calculated MR-FOCUSS signals with the dipole signal is greater than with the MEG data that is imaged. In figure 8C, large changes in residual (noise) power are associated with relatively small change in localization error. The percent of total gray mater represented by sources above a 20% threshold (point spread) decreases slightly with increased noise.

Imaging Extended Souces

The signal from the extended source, figure 9 (left panel), was mixed with the 210 sets of MEG sensor noise described in the previous section. The fit of an MR-FOCUSS solution to the extended source visualized in figure 9, was quantified by two methods. The percent overlap of imaged and modeled source activity was quantified by the percent of the imaged activity above threshold that coincided with locations of the extended source. For MR-FOCUSS solutions generated with P = [2.0, 0.1

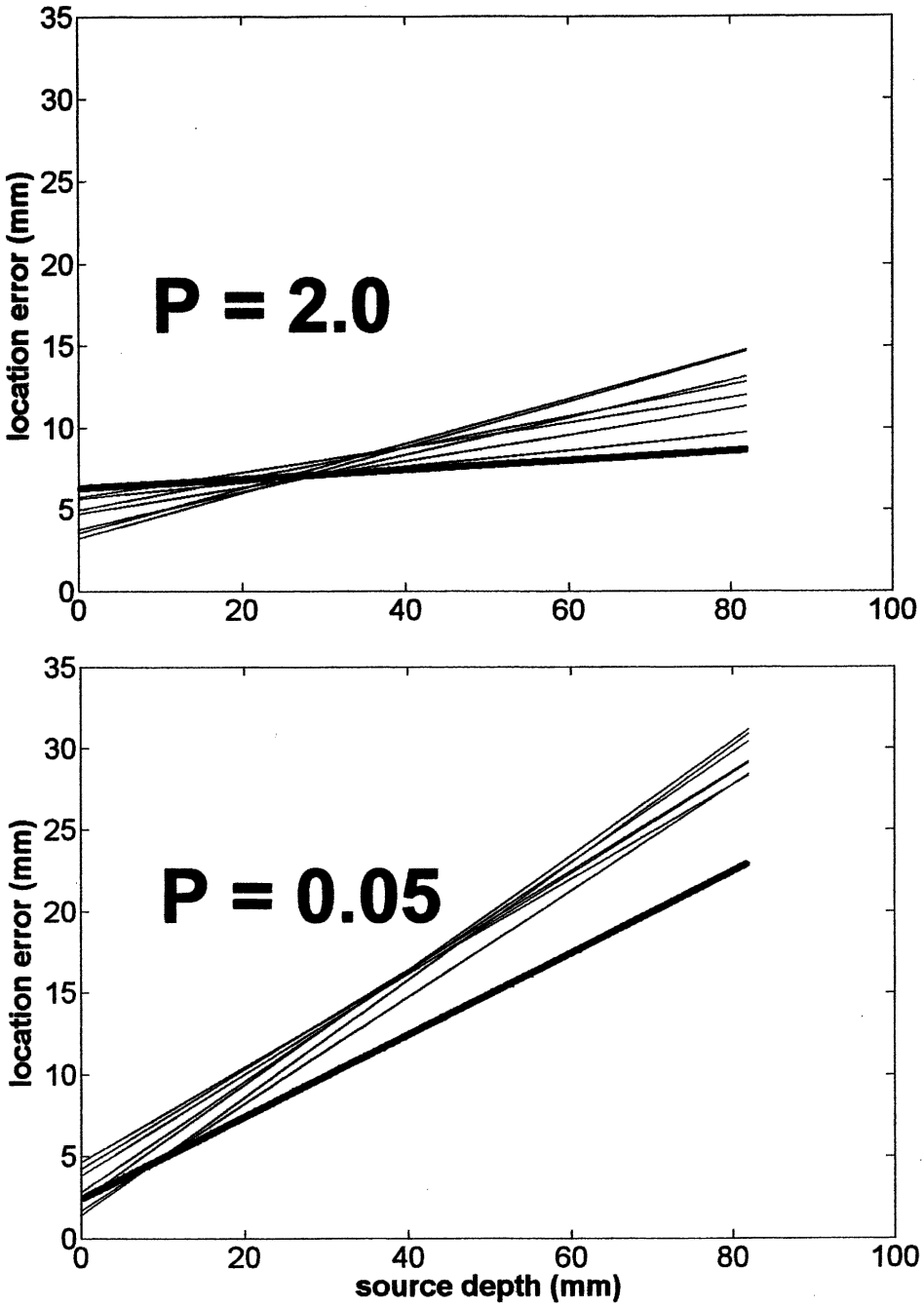

Figure 5. Imaging accuracy of MR-FOCUSS for surface and deep focal sources is altered by the focal imaging parameter P. The performance of MR-FOCUSS with other imaging parameters is between the extremes plotted in this figure. The multiple regression lines correspond to different choices of the minimum solution threshold, 10% (thick line) to 80% of the maximum amplitude.

and 0.05], and a 20% threshold, the overlap of imaged activity on the source model was (78, 94, and 100%). A second measure of fit is the percent of the extended source corresponding to imaged activity. For P = [2.0, 0.1 and 0.05], and a 20% threshold, (51, 35 and 15%) of the modeled source locations exactly matched the imaged activity.

Results: Cortical Language Processing

Language processing is a complex task that involves both sequential and simultaneous cortical activity in language specific regions of the brain. The results presented are from an ongoing study (Bowyer et al. 2004). MEG data were collected from 18 right-handed control subjects

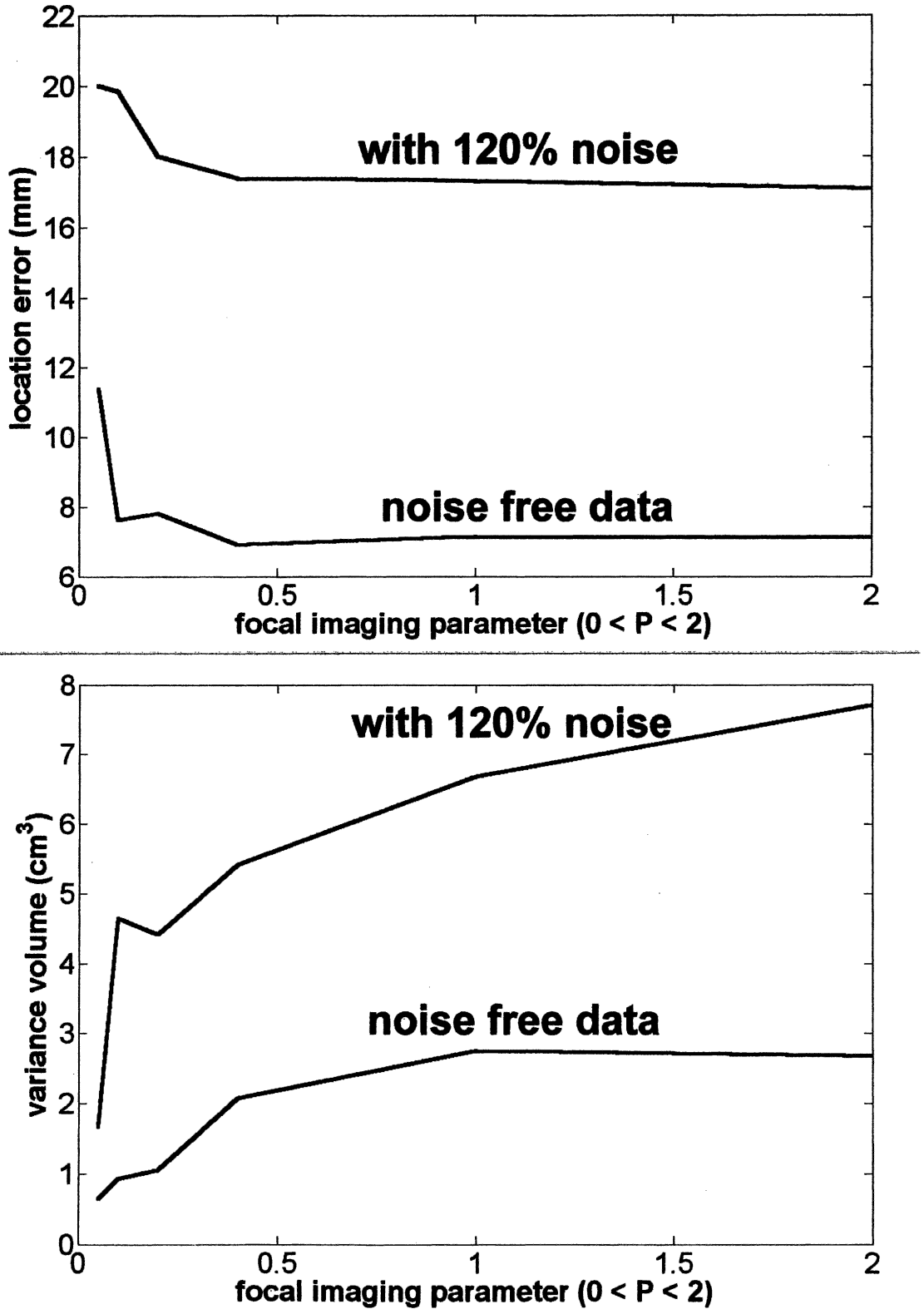

Figure 6. For MEG data including 120% noise, MR-FOCUSS imaging error increased from 7 to 17 mm. The point spread, quantified by the variance volume, increased by a similar amount. Imaging results for surface and deep sources were averaged for this figure.

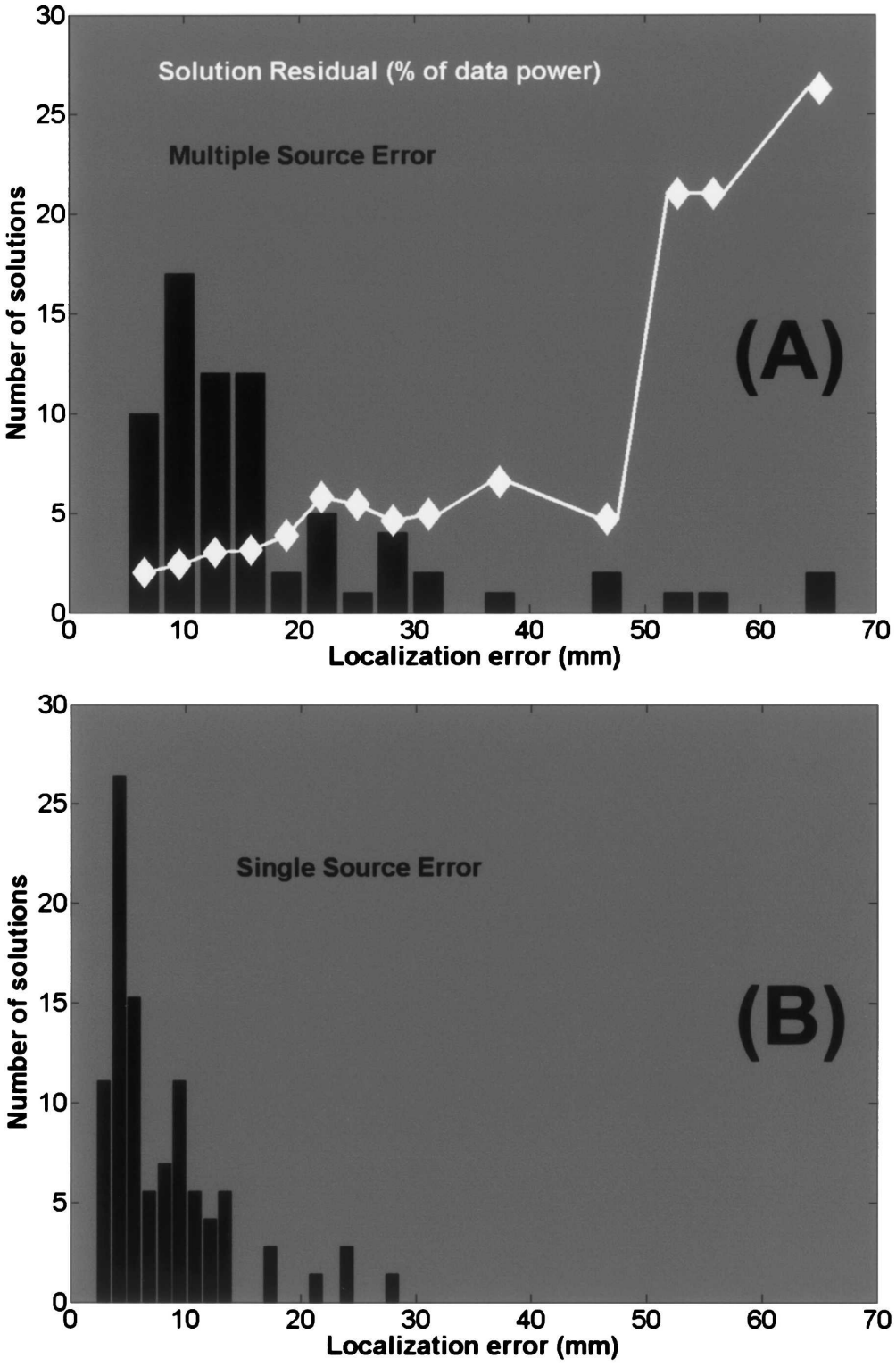

Figure 7. The average multiple source localization error of 71 solutions (A) was 18 mm. The largest errors corresponded to complete failure to identify one of the sources. These solutions had high residual error because MR-FOCUSS was unable to modify the initial poor estimate sufficiently to fit the MEG data. The Single source localization error averaged 8 mm for solutions (B). The higher errors corresponded to deep sources.

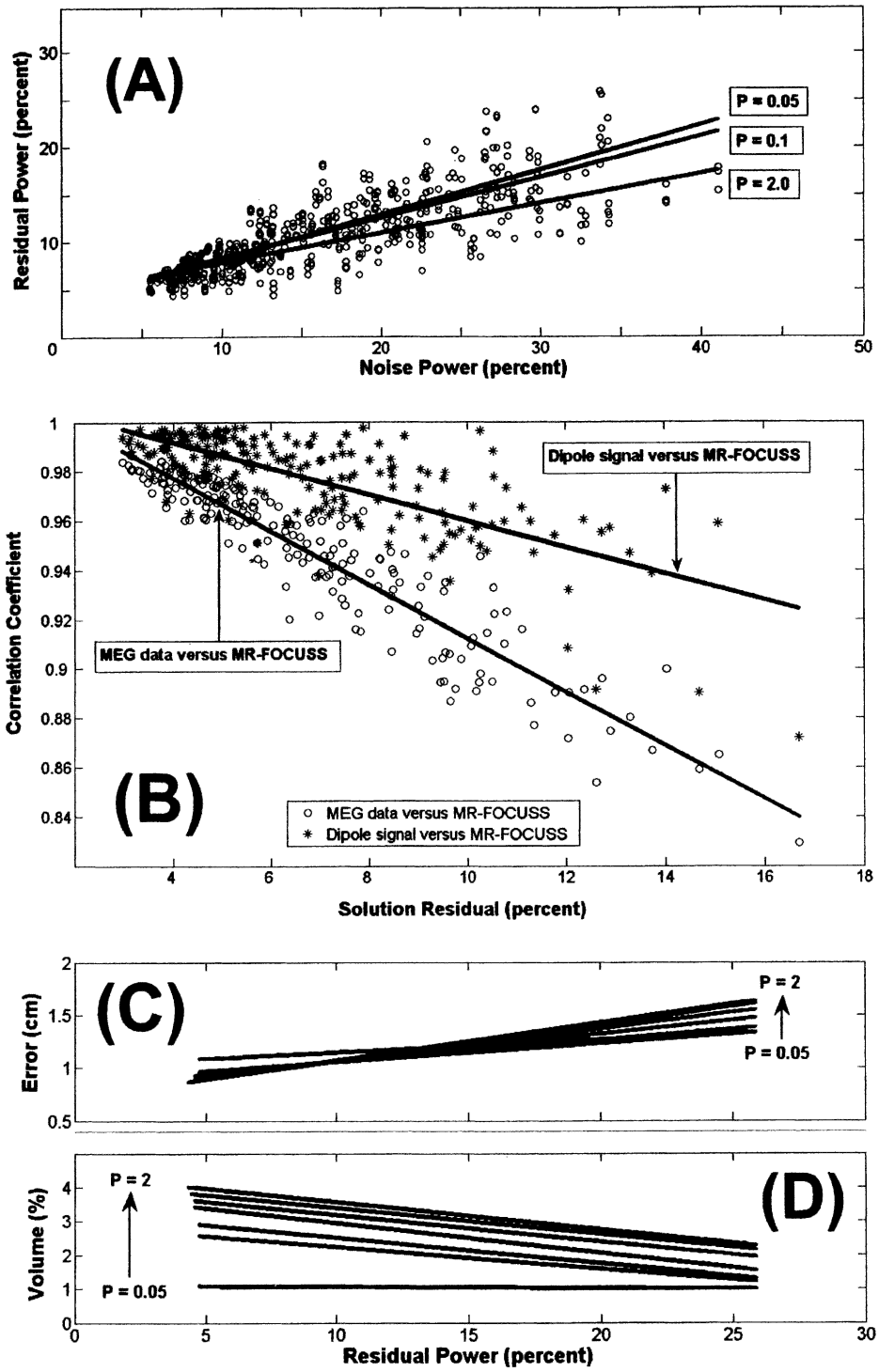

Figure 8. The fraction of the MEG data not imaged increases proportional to the amount of real sensor noise and artifact (A). Therefore, the signal of imaged activity matches the dipole signal better than the MEG data that is imaged (B). Localization error increases by 1 cm when the residual power increases from 5 to 25% of data power (C). The volume of cortex included in the solution (point spread), decreases slightly with increased noise (D).

and 24 right-handed, epileptic patients performing the verb generation task described earlier. For MR-FOCUSS images of these subjects performing the verb generation task, maximum activation in the superior temporal gyrus (STG) and planum temporale occurred at 239 ± 31 ms after visual presentation of the noun. Maximum activation

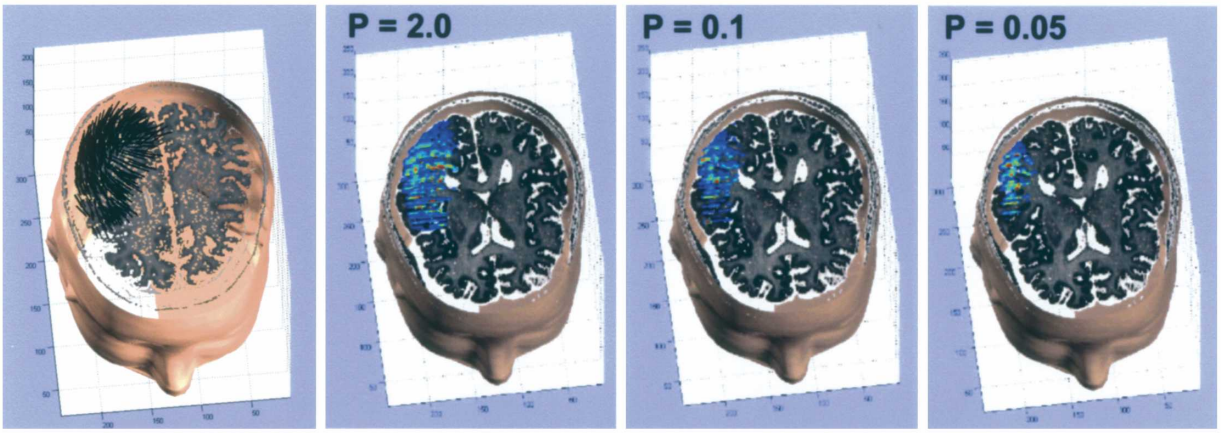

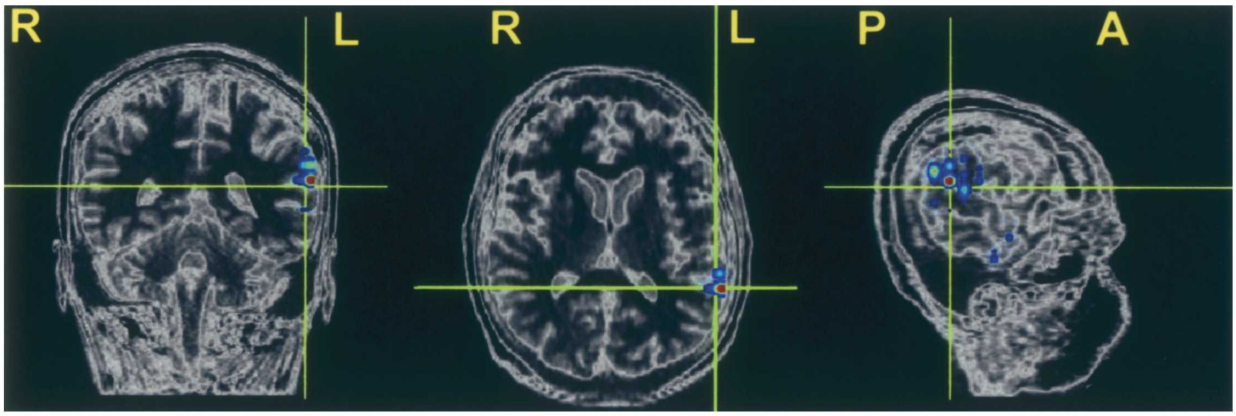

Figure 9 (Top). The extended source was modeled by 270 dipoles. The lines in the figure correspond to the orientation of each source (left). The region including sources above a threshold of 20% of maximum single source amplitude is large for the MR-FOCUSS solution generated with the imaging parameter, P = 2.0, and significantly smaller for imaging parameter, P = 0.05.

Figure 10 (Bottom). In this example of MR-FOCUSS imaging of cortical language processing (Verb Generation Task), the maximum response in the superior temporal gyrus (STG) occurred 247 ms after visual presentation of noun stimulus. Red represents the most intense cortical activation. Blue corresponds to 20% of the maximum amplitude in the red region.

in the lateral prefrontal cortex (PFC) occurred later at 436 ± 40 ms. These results are consistent with other language mapping studies (Helenius et al. 1998; Levelt et al. 1998). Figure 10 depicts the MR-FOCUSS image of peak cortical activation in the left STG for one subject at 247 ms after stimulus onset. The MRI slice display format of figure 10 is useful for relating functional locations to border zones and regions of eloquent tissue when MEG studies are requested for use in surgical planning.

Discussion

Rank ordered mapping of sources onto a partial wavelet decomposition matrix, **P**, differentiates MR-FOCUSS from other imaging techniques. This is a non-linear order statistic filtering operation (Haweel and Clarkson 1992; Fu et al. 1994; Flaig et al. 1998) that minimizes noise sensitivity and provides control over the focal nature of the imaging results. The studies of MR-FOCUSS imaging performance show that additional noise regularization is not required.

MR-FOCUSS and other current density imaging techniques require an initial estimate of cortical activity in which truth is sufficiently represented. Therefore, when available, it is useful to utilize other prior knowledge of cortical activity to construct the initial estimate of cortical activity. This is a major motivating factor for integrating fMRI and PET images of activation as func-

tional constraints for MEG imaging. To increase the likelihood of including the real solution, evaluations of MR-FOCUSS in this study were initialized with a very low-resolution estimate of cortical activation produced by the single current dipole metric. The results show MR-FOCUSS imaging accuracy was relatively high with this initialization and that imaging failure can be identified by the associated high residual power. Initialization bias error can be avoided by initializing MR-FOCUSS with random source amplitudes. However, this strategy requires averaging multiple solutions to obtain each MR-FOCUSS image of activity.

While MR-FOCUSS images a single instance of MEG array data, temporal differences of source activity can be used to enhance imaging both spatial locations of sources and the time course of their signals. This can be achieved by using covariance based MEG imaging techniques such as Multiple Signal Classification (MUSIC) (Mosher et al. 1992; Mosher et al. 1999; Mosher and Leahy 1999) and noise normalized beamformers (Sekihara et al. 2001) to create initial estimates of source activity. However, even greater gains of MR-FOCUSS imaging performance and efficiency are obtained by preprocessing the MEG data with an ICA (Independent Component Analysis) source separation technique (Moran et al. 2004). These MEG-ICA field patterns often correspond to signals from one or a few spatially distinct sources, which can be imaged accurately using MR-FOCUSS as implemented in this imaging evaluation.

We have used MR-FOCUSS in MEG imaging studies of Epilepsy, sensory and motor activity and language processing. In particular, MR-FOCUSS provides a high-resolution method to image sequential activation of multiple correlated sources involved in language processing. Determining locations of important functional regions is particularly important when surgery is being considered or is required. To facilitate these studies, we have developed a complete MEG imaging software package that can be obtained, at no cost, from our website (Moran and Tepley 2005). In addition to MR-FOCUSS, the software includes tools for data visualization, import of MRI volumetric data, construction of a three dimensional head model and cortical model with approximately 3500 points distributed to match the distribution of cortical gray mater extracted from MRI data. The gain matrix, **G**, is calculated for the sources. Solutions can be displayed in MRI overlay or 3D formats and movie sequences can be created for imaging results. Graphical interfaces are used for all data import, processing and display of data as well as imaging using MR-FOCUSS and other techniques.

Appendix

Construction: Multiresolution Basis Vectors

The MR-FOCUSS wavelet vectors are created using the statistical distribution of an imaging metric template, $\mathbf{M_P}(z) = \left| Ae^{-|Z|^p}, 0 \le p \le 2 \right|$. The coefficient, P is specified such that the focal imaging properties of MR-FOCUSS are matched to the imaging task. For the density distribution, $\mathbf{M_P}(z)$, plotting the amplitudes, $[z_j, j = 1,.., N]$, (horizontal axis) versus element rank order, $\mathbf{N} = [1,..,N]$, (vertical axis) creates a cumulative distribution graph, $\mathbf{N}(z)$, with the element rank order represented as a function of the metric amplitude. Alternatively, the cumulative distribution can be represented as $\mathbf{Z}(\mathbf{N})$, where the metric amplitude is a function of the rank order of the elements. The second representation of the cumulative distribution is used in MR-FOCUSS. In figure 11, the vertical lines mark the borders of eight equal intervals of the metric amplitude range, (horizontal axis) resolved by the first four octaves of a Haar wavelet transform [48] of $\mathbf{N}(z)$. However, the grouping of sources along the vertical axis, determined by the corresponding horizontal lines in figure 11, is required for MEG imaging. It is important to note that sources with large amplitudes are in much smaller groupings, (high resolution). A Haar transform of the cumulative distribution with respect to source amplitude, $\mathbf{N}(z)$, (along the horizontal axis) is equivalent to a MR-FOCUSS wavelet transform of the cumulative distribution with respect to source index, $\mathbf{Z}(\mathbf{N})$, (along the vertical axis). For MEG imaging, sources are easily mapped to these MR-FOCUSS wavelets, **P**, by reordering the gain matrix, **G**, and source vector, $\mathbf{q}^{(i)}$, according to the rank order of the imaging metric, $\mathbf{q}^{(i)}_{rq}$, that is updated each recursive step. Additional details of the construction of the MR-FOCUSS wavelet basis, $\mathbf{P} = [\mathbf{P}_0, \mathbf{P}_1, .., \mathbf{P}_L]$, from $\mathbf{M_P}$ is is described in the 2DII reference(Moran and Tepley 2000).

The assignment of sources to these wavelets creates a set of 8 multiresolution source structures. $[\mathbf{q}_k = \mathrm{diag}(\mathbf{q}^{(i)})\mathbf{p}_k, k = 0, .., 7]$, where $\mathbf{q}^{(i)}$ has been placed in rank order of imaging metric amplitudes, $\mathbf{q}^{(i)}_{rq}$, and each $\mathbf{q}_k$ has a gain vector $\mathbf{g}_{Qk} = \mathbf{G}\mathrm{diag}\left(\mathbf{q}^{(i)}\right)\mathbf{P}_k\mathbf{g}_{Qk}$. These multiresolution gain matrix vectors, $\mathbf{G}_Q = [\mathbf{g}_{Q0},.., \mathbf{g}_{Qk},.., \mathbf{g}_{Q7}]$, have quadrupole characteristics because the wavelet structures alter the contribution of one set of sources relative to another set of sources. Good noise rejection and spatial resolution are obtained by using only four octaves of wavelets (8 wavelet vectors). Using 16 wavelet vectors slows MR-FOCUSS calculations significantly without altering the results. With 4 wavelets, spatial resolution is often degraded.

For an N dimensional vector space, the N by N multiresolution basis, $\mathbf{P} = [\mathbf{P}_0, \mathbf{P}_1, .., \mathbf{P}_N]$, is a complete orthonormal basis with:

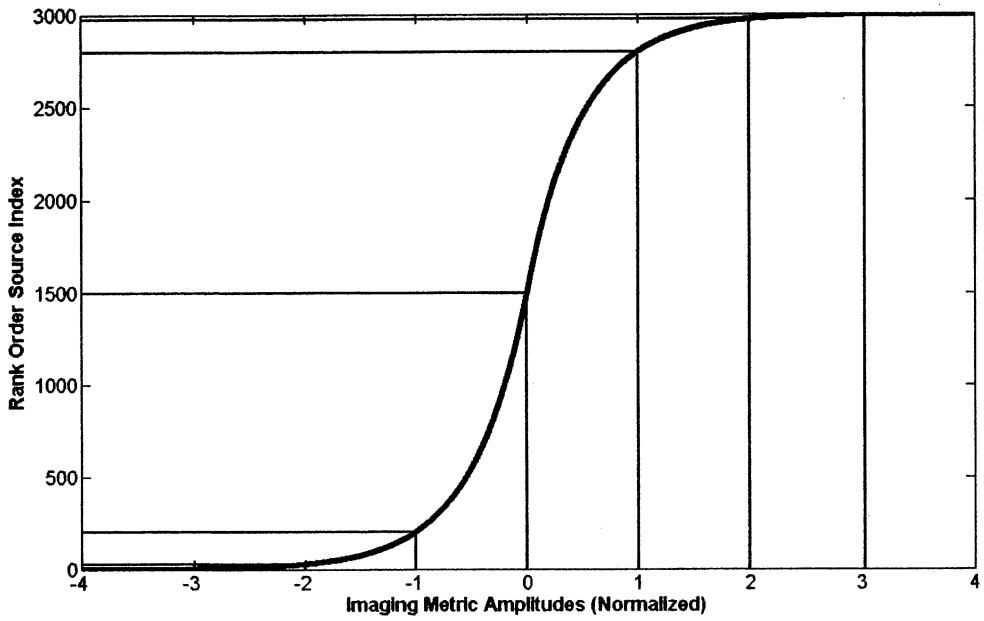

Figure 11. The cumulative distribution of imaging metric amplitudes is shown for the generalized Gaussian distribution, (P = 1.0). The vertical lines correspond to segments of the distribution resolved by four octaves of a Haar wavelet transform with respect to the metric amplitude axis. The horizontal lines show the corresponding non-uniform MR-FOCUSS wavelet division of the cortical sources.

$$\mathbf{P}^T\mathbf{P}=\mathbf{I}_N=\mathbf{P}\mathbf{P}^T$$

$\mathbf{I}_N$ is an N by N identity matrix

For the low resolution subspace, $\mathbf{P} = [\mathbf{P}_0, \mathbf{P}_1, \ldots, \mathbf{P}_L]$, with L < N, the matrix relationships become:

$$\mathbf{P}^T\mathbf{P} = \mathbf{I}_L$$

$\mathbf{I}_L$ is an L by L matrix

$$\mathbf{P}\mathbf{P}^T = \begin{pmatrix} \begin{pmatrix} \frac{1}{m_1} & \cdots & \frac{1}{m_1} \\ \vdots & \ddots & \vdots \\ \frac{1}{m_1} & \cdots & \frac{1}{m_1} \end{pmatrix} & & 0 & & 0 \\ & \ddots & & & \\ 0 & & \ddots & & 0 \\ & & & & \\ & & 0 & & \begin{pmatrix} \frac{1}{m_L} & \cdots & \frac{1}{m_L} \\ \vdots & \ddots & \vdots \\ \frac{1}{m_L} & \cdots & \frac{1}{m_L} \end{pmatrix} \end{pmatrix}$$

$m_1,\ldots,m_L$ are the number of element in structures at finest resolution level

Current Dipole Metric Initialization

MR-FOCUSS requires an initial estimate of cortical activity, $\mathbf{q}^{(0)}$, which is subsequently modified by the MR-FOCUSS algorithm until the residual field has been significantly depleted of signal. Thus, it is important to use a good estimate of the true source distribution for $\mathbf{q}^{(0)}$, which is based on the maximum amount of prior information of brain activity. Some prior information can be implemented as a binary statistical constraint. For example, in our MR-FOCUSS implementation, the cortical model is constructed such that sites within cortical gray mater have a 100% probability of being capable of generating MEG signals and all other locations have 0% probability. However, the x,y,z amplitudes, $\mathbf{q}_k = (q_{kx}, q_{ky}, q_{kz})$, for these gray mater source locations must be estimated using other imaging techniques then modified by an estimate of $P(\mathbf{q}_k \mid \mathbf{b}, \theta)$, the probability of $\mathbf{q}_k$ activity given the MEG data, $\mathbf{b}$ and other prior information parameters, θ. For example, θ could be the orientation of the source relative to the cortical surface or an fMRI activation z-score. Typical, only other MEG imaging techniques are used to calculate an initial estimate of activity, $\mathbf{q}_k$, for each cortical model location. Then, Bayes' rule can be used to calculate $P(\mathbf{q}_k \mid \mathbf{b})$ such the MR-FOCUSS initialization becomes:

$$q^{(0)} = P(b|q_k) \cdot P(q_k) \cdot [q_k, k = 1, L, N]$$

where

$$P(q_k|b) = \frac{P(b|q_k) \cdot P(q_k)}{P(b)} \quad \text{Bayes' Rule}$$

$P(b)$ = normalization constant

For the MR-FOCUSS imaging results in this paper, an initial estimate of q_k for each source location was obtained using a best-fit single equivalent current dipole (ECD) in a spherical conductor matched to the local skull curvature. These calculated ECD amplitude tend to be large for sources deep in the brain and relatively small for those near the cortical surface due to the approximate inverse distance squared relationship between source amplitude and magnetic field strength measured by a magnetometer detector. However, real probability distribution of brain activity amplitudes, $P(q_k)$, is expected to be independent of location. If independent cortical sources are composed of randomly active neurons with stable average firing rates then the probability, $P(q_k)$, is a Poisson distribution. For the MR-FOCUSS technique a Poisson distribution model of $P(q_k)$ was approximated by a Normal distribution with the same mean and standard deviation as the calculated ECD amplitudes. Further, for each source location the ECD correlation coefficient between the MEG data and the forward model of the individual source activity was used as an estimate of $P(b|q_k)$.

References

Baillet, S., Mosher, J.C. and Leahy, R.M. Electromagnetic brain mapping. IEEE Signal Processing Magazine, 2001, 18(6): 14–30.

Bowyer, S.M., Moran, J.E., Mason, K.M., Constantinou, J.E., Smith, B.J., Barkley, G.L. and Tepley, N. MEG localization of language specific cortex utilizing MR-FOCUSS. Neurology, 2004, 6: 2247–2255.

Dale, A.M., Liu, A.K., Fischl, B.R., Buckner, R.L., Belliveau, J.W., Lewine, J.D. and Halgren, E. Dynamic statistical parameteric mapping: combining fMRI and MEG for high-resolution imaging of cortical activity. Neuron, 2000, 26: 55–67.

Darvas, F., Pantazis, D., Kucukaltun-Yildirim, E. and Leahy, R.M. Mapping human brain function with MEG and EEG: methods and validation. NeuroImage, 2004, 23: S289–S299.

Flaig, A., Arce, G.R. and Barner, K.E. Affine order-statistic filters: "medianization" of linear FIR filters. IEEE Transactions on Signal Processing, 1998 46(8): 2101–2112.

Fu, Y., Williamson, G.A. and Clarkson, P.M. Adaptive algorithms for non-gaussian noise environments: the order statistic least mean square algorithms. IEEE Transactions on Signal Processing, 1994, 42(11): 2945–2954.

Gavit, L., Baillet, S., Mangin, J.F., Jérémie P. and Garnero, L. A multiresolution framework to MEG/EEG source imaging. IEEE Transactions on Biomedical Engineering, 2001, 48(10): 1080–1087.

Gorodnitsky, I.F., George, J.S. and Rao, B.D. Neuromagnetic source imaging with FOCUSS: a recursive weighted minimum norm algorithm. Electroencephal. Clin. Neurophysiol., 1995, 95: 231-251.

Gorodnitsky, I.F. and Rao, B.D. Sparse signal reconstruction from limited data using FOCUSS: a re-weighted minimum norm algorithm. IEEE Transactions on Signal Processing, 1997, 45(3): 600–616.

Hämäläinen, M., Hari, R., Ilmoniemi, R., Knuutila, J. and Lounasmaa, O. Magnetoencephalography. Theory, instrumentation and applications to the noninvasive study of human brain function. Rev. Mod. Phys., 1993, 6: 413–497.

Hanson, R. and Swithenby, S.J. The Bassian Power Imaging (BPI) Method for Magnetic Source Imaging. In: J. Nenonen, R.J. Iimoniemi and T. Katila (Eds.), Biomag2000, Proc. 12th int. Conf. On Biomagnetism (Helsinki Univ. of Technology, Espoo, Finland) 2001: 701–704.

Haweel, T.I. and Clarkson, P.M. A class of order statistic LMS algorithms. IEEE Transactions on Signal Processing 1992, 40(1): 44–53.

Helenius, P., Salmelin, R., Service, E. and Connolly, J. Distinct time courses of word and context comprehension in the left temporal cortex. Brain, 1998, 121: 1133-1142.

Horwitz, B. and Poeppel, D. How can EEG/MEG and fMRI/PET data be combined? Human Brain Mapping, 2002, 17(1): 1–3.

Leahy, R.M., Mosher, J.C., Spencer, M.E., Huang, M.X. and Lewine, J.D. A study of dipole localization accuracy for MEG and EEG using a human skull phantom. Electorencephal. clin. Neurophysiology, 1998, 107: 159–173.

Levelt, W., Praamstra, P. and Meyer, A. A MEG study of picture naming. Journal of Cognitive Neuroscience, 1998, 10(5): 553-567.

Liu, A.K., Belliveau, J.W. and Dale, A.M. Spatiotemporal imaging of human brain activity using functional MRI constrained magnetoencephalography data: Monte Carlo simulations. Proc. Natl. Acad. Sci. USA, 1998, 95: 8945-8950.

Liu, A.K., Dale, A.M. and Belliveau, J.W. Monte Carlo simulation studies of EEG and MEG localization accuracy. Human Brain Mapping, 2002, 16: 47-62.

Moran J.E., Tepley N., Two Dimensional Inverse Imaging of Current Sources in Magnetoencephalography, Brain Topography 2000, 12(3) 201–217.

Moran, J.E. and Tepley, N. Source space minimization technique for MEG source analysis. In: J. Nenonen, R.J. Ilmoniemi and T. Katila (Eds.), Biomag2000, Proc. 12th Int. Conf. on Biomagnetism, (Helsinki Univ. of Technology, Espoo, Finland) 2001: 674–676.

Moran, J.E., Bowyer, S. and Tepley, N. Multi-resolution FOCUSS source imaging of MEG data. In: G. Fischer and F.X. Roithinger (Eds.), Proceeding of NFSI 2001. Biomedizinische Technik, 2001, 46(2): 112–114.

Moran, J.E. and Tepley, N. MEG_Tools for MATLAB: MEG im-

aging and Visualization Software, 2005, available at: http://www.megimaging.com.

Moran, J.E., Drake, C.L. and Tepley, N. ICA methods for MEG imaging. Neurology and Clinical Neurophysiology, 2004: 72 (http://www.aacnonline.com/).

Mosher, J.C., Lewis, P.S. and Leahy, R.M. Multiple dipole modeling and localization from spatio-temporal MEG data. IEEE Transactions on Biomedical Engineering, 1992, 39(6): 541-557.

Mosher, J.C., Leahy, R.M. and Lewis, P.S. EEG and MEG: forward solutions for inverse methods. IEEE Transactions on Biomedical Engineering, 1999, 46(3): 245–259.

Mosher, J.C. and Leahy, R.M. Source localization using recursively applied and projected (RAP)MUSIC. IEEE Transactions on Signal Processing, 1999 47(2): 332–340.

Okada, J.C., Huang, J. and Xu, C. A hierachical minimum norm estimation method for reconstructing current densities in the brain from remotely measured magnetic fields. In: M. Hoke, S.N. Erné, Y.C. Okada and G.L. Romani (Eds.), Biomagnetism: Clinical aspects, 8th international conference on Biomagnetism. Elsevier, 1992: 729–734.

Rao, B.D. and Kreutz-Delgado, K. An affine scaling methodology for best basis selection. IEEE Transactions on Signal Processing, 1999, 47(1): 187–200.

Rao, B.D., Engan, K., Cotter, S.F., Palmer, J. and Dreutz-Delgado, K. Subset selection in noise based on diversity measure minimization. IEEE Transactions on Signal Processing, 2003, 51(3): 760–770.

Schmidt, D.M., George, J.S. and Wood, C.C. Bayesian inference applied to the electromagnetic inverse problem. Human Brain Mapping, 1999, 7(3): 195–212.

Sekihara, K., Nagarajan, S.S., Poeppel, D., Marantz, A. and Miyashita, Y. Reconstructing spatio-temporal activities of neural sources using an MEG vector beamformer technique. IEEE Transactions on Biomedical Engineering, 2001, 48(7): 760–771.

Uitert, R. and Van Johnson, C. Can a Spherical Model Substitute for a Realistic Head Model in Forward and Inverse MEG Simulations? In: H. Nowak, J. Hauesen, F. GieBler and R. Huonker (Eds.), Biomag 2002 Proceedings of the 13th International Conference on Biomagnetism (Verlag), 2002: 798–800.

van den Broek, S.P., Reinders, F., Donderwinkel, M., andPeters, M.J. Volume conduction effects in EEG and MEG. Electroencephal. Clin. Neurophysiology, 1998, 106: 522–534.